Securing Robot-assisted Minimally Invasive Surgery through Perception Complementarities

Yun-Hsuan Su
Dept. of Computer Science
Mount Holyoke College
South Hadley, MA 01075
Email: msu@mtholyoke.edu

Yana Sosnovskaya[1] and Blake Hannaford[2]
Dept. of Electrical and Computer Engineering
University of Washington
Seattle, WA 98105
Email: {ysos[1], blake[2]}@uw.edu

Kevin Huang
Dept. of Engineering
Trinity College
Hartford, CT 06106
Email: kevin.huang@trincoll.edu

***Abstract*—Laparoscopic surgery presents practical benefits over traditional open surgery, including reduced risk of infection, discomfort and recovery time for patients. Introducing robot systems into surgical tasks provides additional enhancements, including improved precision, remote operation, and an intelligent software layer capable of filtering aberrant motion and scaling surgical maneuvers. However, the software interface in telesurgery also lends itself to potential adversarial cyber attacks. Such attacks can negatively effect both surgeon motion commands and sensory information relayed to the operator. To combat cyber attacks on the latter, one method to enhance surgeon feedback through multiple sensory pathways is to incorporate reliable, complementary forms of information across different sensory modes. Built-in partial redundancies or inferences between perceptual channels, or perception complementarities, can be used both to detect and recover from compromised operator feedback. In surgery, haptic sensations are extremely useful for surgeons to prevent undue and unwanted tissue damage from excessive tool-tissue force. Direct force sensing is not yet deployable due to sterilization requirements of the operating room. Instead, combinations of other sensing methods may be relied upon, such as non-contact model-based force estimation. This paper presents the design of a surgical simulator software that can be used for vision-based non-contact force sensing to inform the perception complementarity of vision and force feedback for telesurgery. A brief user study is conducted to verify the efficacy of graphical force feedback from vision-based force estimation, and suggests that vision may effectively complement direct force sensing.**

***Keywords* — robot-assisted minimally invasive surgery, cybersecurity, perception complementarity, human robot interaction, haptic feedback**

I. Introduction

A. Background

Robot teleoperation exists in numerous real-world applications including munition remediation, industry, space exploration and robotic-assisted minimally invasive surgery (RMIS) to name a few [1], [2], [3], [4]. Remote human operators are able to manipulate robot motion while simultaneously receiving various forms of sensory feedback through a communication channel, e.g. audio, video, and haptic. This sensory feedback is critical to operator awareness, and ideally accurately reflects the remote environment. In deployment of these architectures, security vulnerabilities of these cyber-physical systems and communication channels are real; critical information transfer may be facilitated through publicly available networks or ad-hoc wireless or satellite networks [5].

Despite this, the teleoperation security problem receives cursory attention in the research community. Bonaci et al. systematically analyzed possible cybersecurity attacks against the Raven-II, an advanced teleoperated robotic surgery platform [6], and experimentally evaluated the scope and impacts of each attack [7], [8]. Quarta et al. proposed an attacker model and re-evaluated the safety standards and security challenges in state-of-the-art industrial teleoperated robots [9]. These and other existing research focus on methods to prevent or mitigate the effects of malicious hackers. In particular, typical approaches aim to protect operator commanded robot motion. In contrast to the previously described prior art, this work examines another approach; reconstructing partial sensory feedback to the operator when one or more feedback channels are compromised. Since teleoperation is a bidirectional form of human robot interaction, a comprehensive cybersecurity strategy should focus on information transfer in both directions. It is envisioned that perception complimentarities may afford robustness to such attacks.

B. Contribution

The contributions of this paper can be summarized by the following points

i) introduce the notion of perception complementarities as a partial solution for cybersecurity in RMIS;
ii) simulate the estimation of haptic information via reconstruction and synthesization through vision;
iii) evaluate through user studies sensory feedback through a disparate channel, in this case the use of graphical force feedback from vision based-estimation.

The combination of these three contributions provide insight into cross-verification and multi-pathway transmission of various types of sensory information to enhance RMIS security. Should one type of sensory information be temporarily compromised, distorted or otherwise absent due to adversarial cyber attacks, inconsistency can be detected and thus addressed via perception complementarities.

This work was supported by the University of Washington as part of the EE589 Advanced Topics in Sensors and Sensor Systems graduate level course.

978-1-7281-5237-0/20/$31.00 ©2020 IEEE
DOI 10.1109/IRC.2020.00013

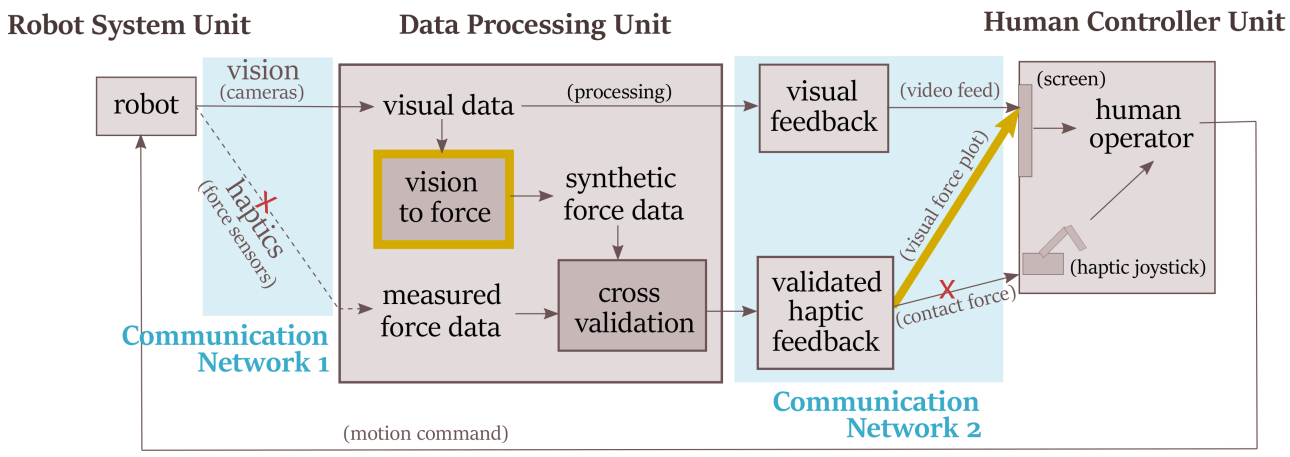

Fig. 1. Teleoperated RMIS architecture with cybersecurity vulnerabilities identified. Two communication networks in the sensory feedback direction are outlined with a blue background. In Communication Network 1, the dashed arrow indicates a sensory input not currently available in state-of-the-art RMIS; other modes of force estimation, e.g. vision-based, are required. Portioned marked in goldenrod highlight the two main areas of research in this work. The red 'X' labels are potential cyber attack pathways in the two communication networks addressed.

C. System Overview

As illustrated in Fig.1, this teloperated RMIS architecture consists of three parts: 1) a remote robotic system unit, 2) a data processing unit and 3) a human controller/operator space. The human operator sends motion commands to the robot, while simultaneously sensory information is relayed from the remote robotic device to the human operator. These transfers of information are facilitated through two separate communication pathways. Cyber attacks can occur in either of these communication networks. In this work, the authors focus on endeavors that have great potential to contribute to verifying information correctness and reconstructing compromised data for cyber attack scenarios occurring in either of the communication networks: sensing and feedback.

1) Perception Complementarity: The two sensory modes of vision and haptics are extremely relevant to surgeons. Both types of sensing are shown in Fig. 1 Communication Network 1. Depending on the type of surgery, visual sensors may include endoscopes, laparoscopes or microscopes, all of which are well tested and utilized in the operating room. However, modern telesurgery still lacks direct force feedback critical to assessing applied force and operation state. This is largely due to the sterilization requirements for surgical tool tips. This lack of force feedback can lead to undesired and unwanted tissue damage [10], [11]. Designing FDA approved force sensors is one approach to solve the problem and an active area of research [12], [13], [14], [15]. In this work, contact force is derived through a simulated vision-based approach.

This vision-based force estimation complements and can be paired with directly/alternatively measured force. If cyber attacks occur in haptic information transmission, the inconsistency can be detected and remediated. This perception complimentarity affords the process of synthesizing one sensory information from another and continual monitoring of sensory consistency, which can address distorted data or temporary information absence due to noise or cyber attacks.

2) Multiple Feedback Channels: Communication Network 2, as depicted in Fig.1, presents another cyber vulnerability. To address this, instead of sending visual feedback through vision and force information through haptic devices, a graphical force plots can be displayed to human operators; namely, the force information is delivered through a disparate pathway. In the user study presented in this work, teleoperators in the simulation were robust to compromised haptic feedback through graphical substitution. Vision-based force estimation and visual feedback thus compensated for degraded complementary force sensing and force feedback. Virtual [16] and graphical force feedback [17] have served as replacements for direct force feedback to varying degrees of success.

II. Methods

In order to address the two goldenrod components in Fig.1, a 2 degree of freedon (DOF) haptic surgical simulator platform with simulated vision sensors was developed. Perception complementarity components were implemented in the sensor portion of the simulation, while feedback channels were consolidated to just visual feedback on the operator side. The graphical user interface of the 2DOF Haptic Surgical Simulator Platform is shown in Fig.2.

A. Simulator Overview

The surgical simulator platform is capable of rendering graphical haptic feedback to the user and compute related physical quantities within the task space. To be specific, the software realistically simulates operations and tool-tissue interaction to provide estimated contact force to human operators via a real time transient graphical force plot. With this, human operators navigate the surgical robot towards a tumor-like target point, as shown as a red circle in Fig. 2. During the simulation, real time analysis of tissue deformation depth, number of collision points, and estimated applied force are displayed graphically. Such parameters are the basis for non-contact vision-based force estimation [18], [19], [20], [21]. In

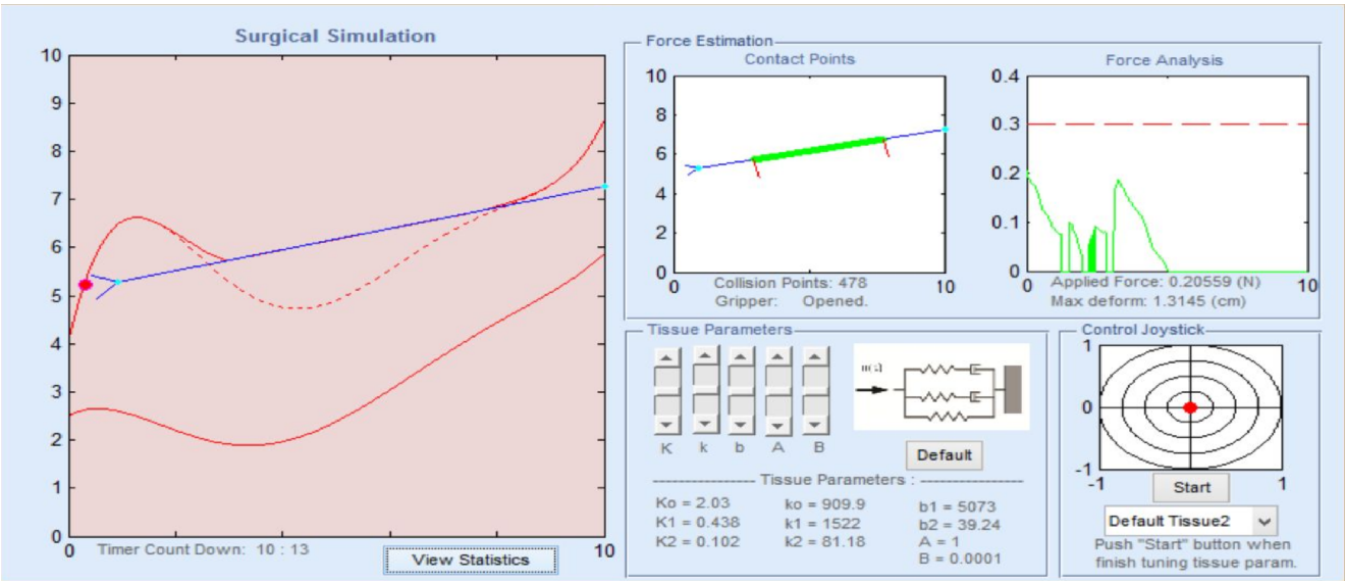

Fig. 2. This is the user interface of the proposed surgical simulator. On the left is the real-time visual feedback of the surgical scene. The top right depicts the estimated force feedback delivered through vision, which consists of contact point detection and a real-time transient visual force plot. The force is determined by tissue deformation analysis combined with the tissue dynamic model, whose parameters are adjustable using five scroll bars. On the bottom right is the surgical tool motion control joystick, where the distance and angle from the circle center respectively determine the direction and speed for the surgical tool. Below that, tissue topology can be selected from several default options or randomly.

terms of force estimation, both tissue mechanics and tool tissue interaction modeling are essential. The nonlinear Wiechert model [22] is adapted for the tissue model, which is capable of estimating applied force given both the level of deformation and deformation rate.

B. Force Rendering from Tissue Dynamics

A mass-spring-damper modelling approach is a simple pragmatic simulation of soft tissue behavior and reactions. Due to the unique material properties of soft tissues, such as anisotropy, viscoelasticity, inhomogeneity, and rheological properties during elongation etc. [23], describing these behavior under manipulation tasks is extremely different than materials more common to industrial or other service robotic applications. In heuristic soft tissue modeling, three basic models are commonly used in terms of viscoelasticity: the KelvinVoigt, the Maxwell and the Kelvin models [24]. Due to the rapid development in the fields of robot control and surgical robotics, more sophisticated models are needed; accuracy requirements of advanced robotic surgical applications are not met by the previously described simple models. In order to incorporate the elastic behavior and stress relaxation more realistically, the Wiechert model is presented and has proven to outperform alternatives [25].

The Wiechert model is composed of mechanical springs and viscous dampers (Fig.3). Force from the spring element is calculated from the spring stiffness value k_i and the deformation of the spring in the longitudinal direction x_i. The reaction force arising in the damper elements is calculated using the damping coefficient value b_i and the rate of deformation of the damper element. However, to realistically model nonlinearities in real tissue, the dynamic model must be modified. To that end, the stiffness values k_i of the spring elements are nonlinear functions of the elongation x_i to reflect the tissue rheological heuristic model.

This model gives a reliable approximation of soft tissue behavior in the force relaxation phase. To create such a model, some basic restrictions are introduced based on two practical considerations, namely

$$k_i\left(x_i\right) \geq 0 \quad \text{and} \quad \frac{d}{dx_i} k_i\left(x_i\right) \geq 0 \quad \forall x_i \geq 0 \tag{1}$$

where $i = 0, 1, 2$. These constraints ensure that both the stiffness values and their derivatives with respect to indentation depths must be non-negative. The proposed nonlinear spring stiffness function is the following:

$$k_i\left(x_i\right) = K_i e^{\kappa_i x_i} \tag{2}$$

The relation between tissue deformation and applied force hence becomes

$$\begin{aligned} f(t) &= k_0(x_0)x_0 + k_1(x_1)x_1 + k_2(x_2)x_2 \\ &= K_0 e^{\kappa_0 x_0} x_0 + K_1 e^{\kappa_1 x_1} x_1 + K_2 e^{\kappa_2 x_2} x_2 \end{aligned} \tag{3}$$

where x_0 is the magnitude of tissue deformation, and x_1, x_2 are the virtual mass points connected to k_1-b_1 and k_2-b_2 in Fig.3 respectively. Compared to the linear Wiechert model which always predicts a concave response curve (constant stiffness parameters), this nonlinear model introduces progressive stiffness and, therefore, has been shown to produce a better fit with real-world data.

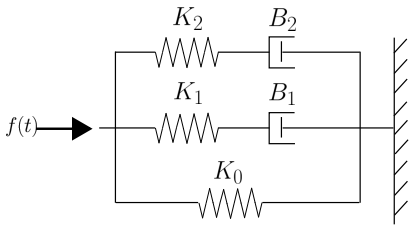

Fig. 3. Wiechert spring damper model of rheological tissue.

C. Tissue Deformation Simulation and Analysis

In order to efficiently apply this model, the deformation paths of terminal points in the combined mechanical elements are required. Provided that this information is given, the force response can be described with a simple mathematical expression. In terms of deformation at the tool tissue contact point, the derivative of x_0, x_1 and x_2 follow the following formulas:

$$\dot{x_0} = v \tag{4}$$

$$\dot{x_1} = \frac{1}{b_1} K_1 e^{\kappa_1 (x_0 - x_1)} (x_0 - x_1) \tag{5}$$

$$\dot{x_2} = \frac{1}{b_2} K_2 e^{\kappa_2 (x_0 - x_2)} (x_0 - x_2) \tag{6}$$

where v is the instantaneous deformation velocity in the longitudinal direction. Combining Eq.(3)-(6), the tissue model requires three inputs (x_0, x_1, x_2) and generates output contact force $f(t)$. Meanwhile, it yields a total of eight unknown parameters (k_0, k_1, k_2, κ_0, κ_1, κ_2, b_1, b_2), to provide realistic tissue behavior in both relaxation and compression phases for reaction force estimation.

In reality, the tool tissue contact point is not the only point where the tissue might deform, instead the neighboring tissue patches do as well. Suppose $\hat{x_0}$ is the level of tissue deformation at the contact point. Then any neighboring points that are a distance $d < \rho$ away from the tool tissue interaction point will deforming by $x_0(d)$, which is defined as Eq.(7). Neighboring points outside the finite distance limit of ρ are considered unaffected.

$$x_0(d) = \frac{\hat{x_0}}{\rho^2} (|d| - \rho)^2, \forall d \leq \rho \tag{7}$$

where ρ is heuristically tuned, and for this work is 16 mm. Figure4 illustrates example simulated tissue deformation at 11 mm of indentation depth. On the left, Eq.(7) is not applied whereas on the right Eq.(7) is adopted.

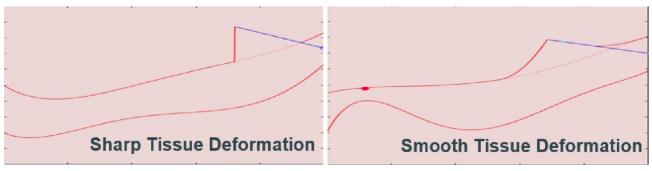

Fig. 4. An illustration of local tissue patch deformation with and without using Eq.(7). The simulator adopts the smooth tissue deformation scheme, which makes use of Eq.(7).

D. Simulator Interface Design

As shown in Fig.2, there are four distinct sections of the graphical user interface: 1) Surgical Simulation, 2) Force Estimation, 3) Tissue Parameters, and 4) Control Joystick. These are described below.

1) Surgical Simulation: During the simulation, red dotted lines represent the boundary of the tissue geometry, while blue lines represent the surgical tool. The solid red line represents tissue deformation and the distance calculations are carried out based on deformation level. A timer signals a 30 second countdown for each trial. During the simulation, users can press key "g" to actuate the surgical tool gripper. When the surgical robot reaches the target position, the gripper must open in order to complete the task. At the completion of any trial, a "View Statistics" option displays performance.

2) Force Estimation: Force estimation is displayed in the section located in the upper right of Fig.2, and contains two subplots: "Contact Points" and "Force Analysis". "Contact Points" plots and keeps track of the tool-tissue interaction, and marks the collision points in green using small red line segments to indicate direction of force. The number of collision points are also quantified by discretizing the tissue geometry into a list of points spaced 0.1 mm apart. "Force Analysis" plots the total force applied in real time. If the applied force exceeds the maximum allowed force (set to 0.3N), then the trial is terminated and considered a failure. Before each trial, the user may press the "f" key to toggle whether or not to display the visual force plot.

3) Tissue Parameter: The tissue parameters can be manually tuned via five sliders. There is also a convenient button to reset tissue parameters to default values from [23]. Eight tissue parameters are present but a reduction to five are provided in the tunable range. The first three sliders determine the stiffness of the tissue, i.e. how much force is required for the tissue to deform given distances. The final two sliders determine the rate of tissue recovery in the relaxation phase after tool-tissue interaction terminates.

4) Control Joystick: The joystick for user control input for the surgical robot is displayed in the bottom right of the interface. Following adjustments to the tissue parameters, users may initiate the surgical simulation by choosing a tissue geometry type and then clicking the "Start" button. There are a total of five tissue geometries along with a random tissue generation option. By default, a random tissue geometry is selected. Once the simulation starts, the user can move the acuate surgical robot by hovering the cursor around the "Control Joystick" area. The "Control Joystick" area is represented as a radar plot where the orientation of the joystick controls the movement direction of the surgical robot tip. The magnitude of deviation from center determines movement speed; the larger the faster the robot moves. The joystick is only enabled when the simulation starts and is colored blue when enabled and red when disabled.

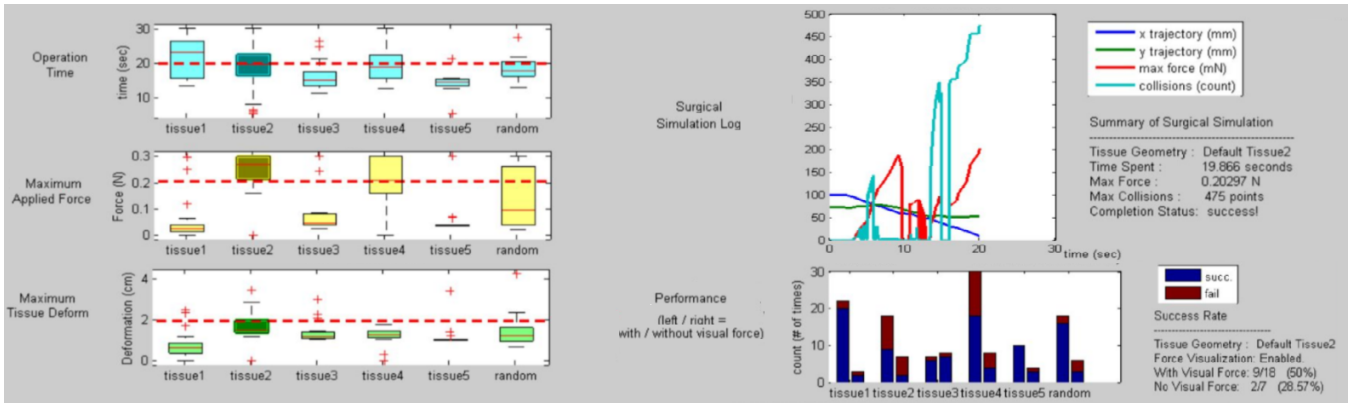

Fig. 5. Online statistics of the simulator. On the left three box plots show user performances in different metrics. The top left shows statistical completion time on each tissue topology, the middle shows the maximum applied force and the bottom left shows maximum tissue deformation. The red dotted line on each of the 3 box plots show the performance of the current user and the darkened "boxes" show the tissue topology chosen in the current trial. On the upper right, a plot displays the trajectories of the gripper; maximum force over time; number of collisions over time. On the bottom right, a bar chart shows the accumulated completion statuses (blue being a successful trial and red stands for failing). For each tissue terrain, the left bar shows results of trials with visual feedback and on the right are trials without visual feedback.

III. User Study Methods

The goal of the simulated telesurgical task is to navigate a surgical robot through a narrow pathway to reach a tumor-like target (marked with a red dot) within 30 seconds while ensuring the contact force remains below a predetermined maximum force threshold.

A. Schematics of the Telesurgical Task

The human operator starts by setting up the simulation parameters, including the tissue properties, the task mode, and a choice of either to hide or reveal the applied force (toggle with keyboard button "f"). The simulator starts with a click of the start button, initiating a 30sec count-down timer. One objective is for the human operator to avoid exceeding the maximum applied force threshold and maximum allowed tissue deformation; otherwise the simulation will terminate in failure. The operator must successfully navigate and open the gripper once the target is reached. If the user successfully finishes the task within the allotted time, applied force and maximum tissue deformation limits, the user can immediately check the accumulated performance statistics of the current trial compared with all previous attempts. There are also two failure cases that terminates the trial before the surgical gripper reaches the target - "Operation Timeout" and "Exceeded Max Allowed Force". All three termination conditions (two failure cases and one success case) are summarized in Fig.6.

B. Real-time Accumulated Statistics

In this project, online statistical data is provided to each human operator after each individual trial is completed. Users can see their performances compared with the accumulated results of all previous human operators. Fig.5 show the statistics of an example trial where tissue 2 was chosen. The user performance was unremarkable in time; applied less force than average; and had more tissue deformation than the average operator.

C. Subject Recruitment and Trial Sequencing

There were a total of 40 human operators recruited from the university campus. All subjects were tasked with performing the telesurgical task on various pre-designed or random tissue topologies - five subjects performed the telesurgery in a controlled sequence of 14 trials shown in Fig.8. The 14 trails were carefully ordered to minimize learning effects. In order to avoid biased result due to the subjects' initial unfamiliarity with the surgical simulator platform and any the potential learning effects of repeated tissue geometry, we allow subjects to test and familiarize themselves on random tissue geometry. Meanwhile, all users were introduced to the same sequence of 14 trials to avoid distinct learning results due to the order in which different tissue geometries were presented.

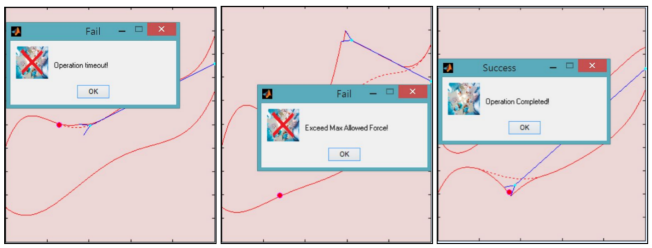

Fig. 6. The three termination scenarios of the telesurgical task and the operator notification.

D. Source Code and Demo Video

The developed software is packaged as a compact surgical simulator platform; the software is open-source. Other researchers may start by watching the demo video here:
https://youtu.be/TQfYROOYnQY
And the code can be downloaded and contributed to in a repository on GitHub at:
github.com/melodysu83/Surgical_Simulator_with_Visual_Force

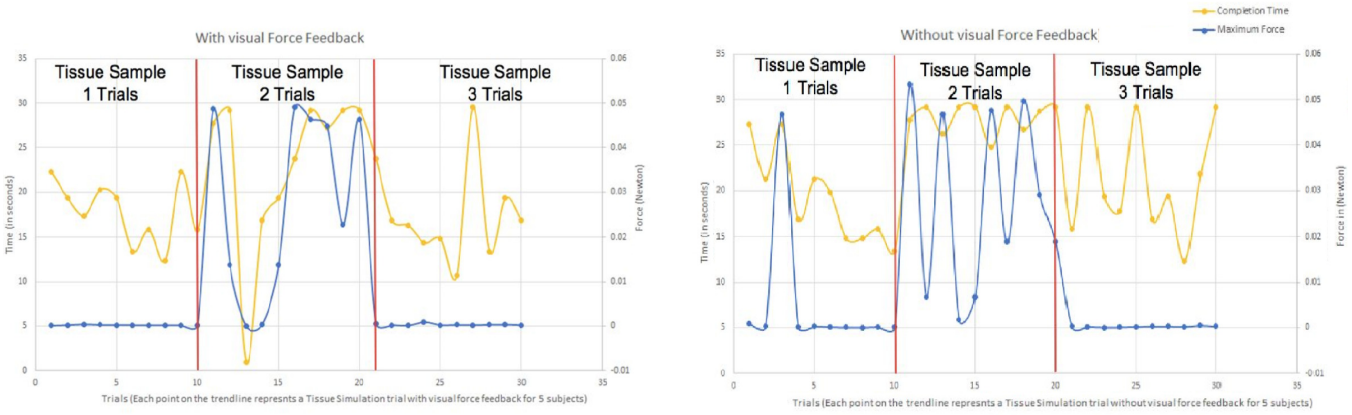

Fig. 7. Completion time and maximum applied force from each trial conducted by the five subjects using different tissue topologies. On the left is trials with visual force feedback and on the right are trials without. The subjects are tasks to perform telesurgeries on each tissue topology four times (two with visual force feedback and two without). There are 10 sample points in each tissue topology category in the left and right subplot. The primary and the secondary y-axes represent completion time (left [secs]) and maximum force force feedback (right [N]).

IV. Results

The statistical data in Fig.7 show positive correlation between the maximum force and the time taken to complete the experiment. However, this is especially true for the trials (sample points on the graph) that are representing the most complex and difficult tissue sample (Tissue Sample 2). For the simpler tissue geometry (Tissue Sample 1), there is little correlation between the completion time and the maximum force feedback. Meanwhile, human operators tend to perform better in both efficiency and applied force with visual force feedback than without visual force feedback. Several users also shared qualitatively that they relied on the visual force plot during situations nearing time limit (30 seconds). As a result, operators needed to act faster while controlling for force or when the tissue geometry is challenging with unavoidable tool-tissue contact.

The bar chart depicting performance in Fig.5 shows a higher success rate with visual force as compared to without. Furthermore, comparing the bar plots among different tissue geometries, the results reflect that having visual force feedback improves the performance more significantly as tissue geometries are more complex and challenging to navigate.

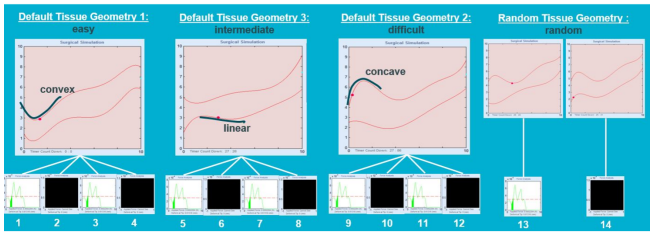

Fig. 8. To normalize learning affects, a controlled sequence of 14 trials were administered. The first four trials were executed using tissue geometry 1, which are conducted alternating between use of and lack of force visualization. Trials number five through eight follow the same procedure using tissue geometry 3, then the same for tissue geometry 2 in trials nine through 12. Finally, trial 13 and 14 are executed using randomly generated tissue geometry, one - with force visualization and the other without.

TABLE I
Performance with and without Visual Force

Visual Force	Without		With	
Success / Tissue	Count	Rate(%)	Count	Rate(%)
Default 1 (easy)	2 / 3	66.66	20 / 22	90.91
Default 2 (hard)	2 / 7	28.57	9 / 18	50.00
Default 3 (medium)	7 / 8	87.50	6 / 7	85.71
Default 4 (medium)	4 / 8	50.00	18 / 30	60.00
Default 5 (hard)	3 / 4	75.00	11 / 11	100.00
Random (-)	3 / 6	50.00	17 / 19	89.47

Results indicate that force feedback results in better operator performance in teleoperation of surgical robots in the surgical simulator. Moreover, an improved performance is shown even when both the generation and display of force sensation are not displayed through haptic sensations - namely, the authors estimated contact forces based on vision instead of direct measurement and realyed the information to human operators through visual plots rather than a haptic joystick. The authors' endeavors on the surgical simulator development and user study afford great potential for incorporating visually displayed vision-based force feedback in future robotic telesurgerical training or operations. This concept lays the groundwork for the greater context of perception complementarity and applications in cybersecurity problems in medical robot teleoperation.

V. Conclusion

Robotic-assisted telesurgery marries the expertise of highly experienced surgeons, the dexterity of machines and the possibility of remote operations for applications in environments such as the battle field or even in outer space. When performing extremely delicate tasks that involve human lives through a vulnerable communication channel, cybersecurity is one of the most critical issues. As mentioned in points ii and iii in Section I-B, and highlighted by the two yellow components in Fig.1, this study proves the effectiveness of (a) generating haptics

from vision and (b) displaying haptics through vision in teleoperated surgical tasks. Both are variations and components of the broader concept of perception complementarity. The former demonstrates the feasibility and prototype of secondary sensory information acquirement pathways apart from direct measurement, while the latter provides an alternative channel to deliver sensory feedback to the human operator. Inconsistency between the primary transmission pathway and the secondary one can serve as an indication of unexpected noise or disturbance to the data. These backup information collection and transmission schemes serve as a novel means to preserve security and robustness of a teleoperated robotic system when one or more information pathways encounter adversarial attacks and experience temporary data loss or distortion. Corresponding procedures such as sensory substitution and reconstruction can be conducted. In future work, the authors are interested in modeling real-world cyber attack scenarios in telesurgical tasks and experiment how the presented techniques in this work can be applied to and provide data reconstruction solutions in such situations.

ACKNOWLEDGMENT

The authors would like to thank Mayuree Binjolkar from the STAR Lab at the Industrial and Systems Engineering Department at the University of Washington for her assistance with the experiments.

REFERENCES

[1] J. Gancet, D. Urbina, P. Letier, M. Ilzokvitz, P. Weiss, F. Gauch, G. Antonelli, G. Indiveri, G. Casalino, A. Birk *et al.*, "Dexrov: Dexterous undersea inspection and maintenance in presence of communication latencies," *IFAC-PapersOnLine*, vol. 48, no. 2, pp. 218–223, 2015.

[2] P. G. De Barros and R. W. Linderman, "A survey of user interfaces for robot teleoperation," *WPI Digital Commons*, 2009.

[3] B. Zhang, H. Staab, J. Wang, G. Q. Zhang, R. Boca, S. Choi, T. A. Fuhlbrigge, S. Kock, and H. Chen, "Teleoperated industrial robots," Sep. 15 2015, uS Patent 9,132,551.

[4] E. Pruna, A. Acurio, I. Escobar, S. A. Pérez, P. Zumbana, A. Meythaler, and F. A. Álvarez, "3d virtual system using a haptic device for fine motor rehabilitation," in *World Conference on Information Systems and Technologies*. Springer, 2017, pp. 648–656.

[5] D. J. Dubois, Y. Bando, K. Watanabe, and H. Holtzman, "Lightweight self-organizing reconfiguration of opportunistic infrastructure-mode wifi networks," in *2013 IEEE 7th International Conference on Self-Adaptive and Self-Organizing Systems*. IEEE, 2013, pp. 247–256.

[6] P. R. D. G. Blake Hannaford, Hawkeye King, "Raven-II: An open platform for surgical robotics research," *IEEE Transactions on Biomedical Engineering*, vol. 60, no. 4, pp. 954–959, 2013.

[7] T. Bonaci, J. Herron, T. Yusuf, J. Yan, T. Kohno, and H. J. Chizeck, "To make a robot secure: An experimental analysis of cyber security threats against teleoperated surgical robots," *arXiv preprint arXiv:1504.04339*, 2015.

[8] T. Bonaci, J. Yan, J. Herron, T. Kohno, and H. J. Chizeck, "Experimental analysis of denial-of-service attacks on teleoperated robotic systems," in *Proceedings of the ACM/IEEE Sixth International Conference on Cyber-Physical Systems*. ACM, 2015, pp. 11–20.

[9] D. Quarta, M. Pogliani, M. Polino, F. Maggi, A. M. Zanchettin, and S. Zanero, "An experimental security analysis of an industrial robot controller," in *2017 IEEE Symposium on Security and Privacy (SP)*. IEEE, 2017, pp. 268–286.

[10] L. Cheng and B. Hannaford, "Evaluation of liver tissue damage and grasp stability using finite element analysis," *Computer methods in biomechanics and biomedical engineering*, vol. 19, no. 1, pp. 31–40, 2016.

[11] S. De, J. Rosen, A. Dagan, B. Hannaford, P. Swanson, and M. Sinanan, "Assessment of tissue damage due to mechanical stresses," *The International Journal of Robotics Research*, vol. 26, no. 11-12, pp. 1159–1171, 2007.

[12] U. Kim, Y. B. Kim, J. So, D.-Y. Seok, and H. R. Choi, "Sensorized surgical forceps for robotic-assisted minimally invasive surgery," *IEEE Transactions on Industrial Electronics*, vol. 65, no. 12, pp. 9604–9613, 2018.

[13] Y. Noh, S. Sareh, E. L. Secco, and K. Althoefer, "Optical force and torque sensor for flexible robotic manipulators," *Soft and Stiffness-controllable Robotics Solutions for Minimally Invasive Surgery: The STIFF-FLOP Approach*, p. 99, 2018.

[14] C. Gaudeni and D. Prattichizzo, "A mathematical model of the pneumatic force sensor for robot-assisted surgery," in *2019 IEEE World Haptics Conference (WHC)*. IEEE, 2019, pp. 598–603.

[15] D.-Y. Seok, Y. B. Kim, U. Kim, S. Y. Lee, and H. R. Choi, "Compensation of environmental influences on sensorized-forceps for practical surgical tasks," *IEEE Robotics and Automation Letters*, vol. 4, no. 2, pp. 2031–2037, 2019.

[16] A. Bettini, P. Marayong, S. Lang, A. M. Okamura, and G. D. Hager, "Vision-assisted control for manipulation using virtual fixtures," *IEEE Transactions on Robotics*, vol. 20, no. 6, pp. 953–966, 2004.

[17] A. M. Okamura, L. N. Verner, T. Yamamoto, J. C. Gwilliam, and P. G. Griffiths, *Force Feedback and Sensory Substitution for Robot-Assisted Surgery*. Boston, MA: Springer US, 2011, pp. 419–448.

[18] Y.-H. Su, K. Huang, and B. Hannaford, "Real-time vision-based surgical tool segmentation with robot kinematics prior," in *2018 International Symposium on Medical Robotics (ISMR)*. IEEE, 2018, pp. 1–6.

[19] ——, "Multicamera 3d reconstruction of dynamic surgical cavities: Camera grouping and pair sequencing," in *2019 International Symposium on Medical Robotics (ISMR)*. IEEE, 2019, pp. 1–7.

[20] Y.-H. Su, I. Huang, K. Huang, and B. Hannaford, "Comparison of 3d surgical tool segmentation procedures with robot kinematics prior," in *2018 IEEE/RSJ International Conference on Intelligent Robots and Systems (IROS)*. IEEE, 2018, pp. 4411–4418.

[21] Y.-H. Su, K. Huang, and B. Hannaford, "Multicamera 3d reconstruction of dynamic surgical cavities: non-rigid registration and point classification," in *2019 IEEE/RSJ International Conference on Intelligent Robots and Systems (IROS)*. IEEE, 2019.

[22] Á. Takács, I. J. Rudas, and T. Haidegger, "Surface deformation and reaction force estimation of liver tissue based on a novel nonlinear mass–spring–damper viscoelastic model," *Medical & biological engineering & computing*, vol. 54, no. 10, pp. 1553–1562, 2016.

[23] A. Constantinesco, H. Schwerdt, and J. Chambron, "Testing device to determine the dynamic rheological properties of soft tissues in biaxial elongation," *Medical and Biological Engineering and Computing*, vol. 19, no. 2, pp. 129–134, 1981.

[24] W. Maurel, Y. Wu, N. M. Thalmann, and D. Thalmann, *Biomechanical models for soft tissue simulation*. Springer, 1998.

[25] X. Wang, J. A. Schoen, and M. E. Rentschler, "A quantitative comparison of soft tissue compressive viscoelastic model accuracy," *Journal of the mechanical behavior of biomedical materials*, vol. 20, pp. 126–136, 2013.